

ON OBLIQUELY MAGNETIZED AND DIFFERENTIALLY ROTATING STARS

XING WEI AND JEREMY GOODMAN

Princeton University Observatory, Princeton, NJ 08544, USA;

xingwei@astro.princeton.edu; jeremy@astro.princeton.edu

Received 2015 January 12; accepted 2015 April 14; published 2015 June 5

ABSTRACT

We investigate the interaction of differential rotation and a misaligned magnetic field. The incompressible magnetohydrodynamic equations are solved numerically for a free-decay problem. In the kinematic limit, differential rotation annihilates the non-axisymmetric field on a timescale proportional to the cube root of magnetic Reynolds number (Rm), as predicted by Rädler. Nonlinearly, the outcome depends upon the initial energy in the non-axisymmetric part of the field. Sufficiently weak fields approach axisymmetry as in the kinematic limit; some differential rotation survives across magnetic surfaces, at least on intermediate timescales. Stronger fields enforce uniform rotation and remain non-axisymmetric. The initial field strength that divides these two regimes does not follow the scaling $Rm^{-1/3}$ predicted by quasi-kinematic arguments, perhaps because our Rm is never sufficiently large or because of reconnection. We discuss the possible relevance of these results to tidal synchronization and tidal heating of close binary stars, particularly double white dwarfs.

Key words: magnetohydrodynamics (MHD) – stars: rotation – white dwarfs

1. INTRODUCTION

Current understanding of stellar differential rotation leaves much to be desired. Centuries of sunspot observations show that the Sun rotates more quickly than its equator. Helioseismology reveals that this latitudinal variation extends throughout the convection zone, but contrary to expectations for a (nearly) isentropic region, the angular velocity is not constant on cylinders (Schou et al. 1998). There is no consensus as to how this pattern is maintained, though the convection itself is presumably essential. Inversions for the radiative core are consistent with uniform rotation down to at least $0.2 R_{\odot}$ (Chaplin et al. 1999); constraints at greater depth are weak because they depend on a few low-degree p modes. Asteroseismological analyses of *Kepler* photometry find that many giants and subgiants have cores that rotate more rapidly than their envelopes, but not so rapidly as if these cores had contracted at constant angular momentum (Deheuvels et al. 2012, 2014; Mosser et al. 2012). Magnetic transport of angular momentum is likely responsible (Maeder & Meynet 2014), but standard prescriptions used by the stellar-evolution community fail to explain the observations quantitatively (Eggenberger et al. 2012; Cantiello et al. 2014). White dwarfs, the end states of low-mass stars, are known to rotate slowly, with periods ranging from hours to days (Berger et al. 2005; Kawaler 2014 and references therein). Asteroseismological attempts to measure *differential* rotation in the interiors of pulsating white dwarfs have so far produced ambiguous results (Charpinet et al. 2009; Corsico et al. 2011). The role of stellar magnetic fields in the transport of angular momentum in all of these objects may be crucial but is not yet well understood. The present work addresses one aspect of this complex problem.

Ferraro’s isorotation law applied to stellar interiors states that “the star can possess a steady field only if the field is symmetric about the axis of rotation, and each line of force lies wholly in a surface symmetric about the axis and rotating with uniform angular velocity” (Ferraro 1937). A detailed derivation can be found in Cowling (1957). The theorem can be mathematically expressed as $\mathbf{B}_p \cdot \nabla \Omega = 0$, where \mathbf{B}_p is the axisymmetric

meridional field and Ω the angular velocity. This formula shows that the contours of the axisymmetric meridional field are parallel to the contours of angular velocity. The isorotation law is strictly valid only for a perfect conductor, i.e., the magnetic Reynolds number $Rm \rightarrow \infty$. Later, Mestel & Weiss (1987) studied the dynamical and resistive effects of departures from the isorotation law. Their results suggest that Alfvén waves transfer angular momentum along meridional field lines—at different speeds on different lines—until the isorotation law is achieved. This mechanism of “phase mixing” was studied by Ionson (1978), Heyvaerts & Priest (1983), and Spruit (1999). The latter estimated that the wave amplitude should decay as $e^{-(t/t_p)^3}$ on a phase-mixing timescale $t_p \sim (R^4/\eta Va^2)^{1/3}$, R being stellar radius, η being magnetic diffusivity, and Va being a typical Alfvén speed. Therefore, it may be inferred that if all field lines are attached to a uniformly rotating solid core, then the entire stellar (or planetary) interior will eventually achieve solid-body rotation (e.g., Charbonneau & MacGregor 1992). Mestel & Weiss (1987) suggested that, even without such a core, a fluid body will tend toward solid-body rotation if its magnetic field is significantly non-axisymmetric: for example, a dipolar field whose axis is not parallel to the rotation axis, a situation referred to in our paper as an *oblique rotator*. It is this last assertion, rather than the whole subject of stellar differential rotation, that is the main focus of the present paper.

Mestel and Weiss perhaps overstated their argument by restricting the velocity field to pure rotation, rather than a combination of rotation and meridional circulation. Consider, for example, a star in a nontrivial state of isorotation aligned with its magnetic axis, but undergoing slow precession around another axis (due, perhaps, to the tidal torque of a companion). Such a star would not be strictly axisymmetric with respect to the axis defined by its total angular momentum, but its velocity field—which would have meridional as well as azimuthal components with respect to that axis—could satisfy Ferraro’s Law and be steady in a frame rotating with the star’s body axes. The calculations described in this paper allow for meridional motions.

Even as Mestel and Weiss posed the problem, the outcome surely depends on the relative strengths of the field and of differential rotation. Rädler (1986) considered the kinematic limit in which the backreaction of the magnetic field on the flow is neglected, so that the field evolves initially linearly according to the induction equation in a prescribed flow. He concluded that the combined effects of differential rotation and magnetic diffusion cause the non-axisymmetric field to decay more rapidly than the axisymmetric field, thus tending to reduce the magnetic obliquity. Allowing for magnetic forces, Mestel (1999, Section 9.3) concluded that a non-axisymmetric meridional field with a weak component perpendicular to the rotational axis can be destroyed by differential rotation, but a stronger perpendicular component can destroy the differential rotation. The principal goal of the present paper is to test and quantify these conclusions by explicit calculations.

The problem posed here has several applications in geophysics and astrophysics. In many stars and fluid planets, it will often be complicated by a magnetic dynamo, which may reinforce the magnetic field in ways that cannot confidently be predicted. We are motivated, however, mainly by applications to white dwarfs, whose magnetic fields are probably relics inherited from their progenitors. The interaction between differential rotation and magnetic fields may therefore be simpler to study in the context of white dwarfs than in main-sequence or red-giant stars. Admittedly the observational constraints are weaker in white dwarfs. On the other hand, the consequences might be more dramatic, as we now explain.

In the double-degenerate scenario for Type Ia supernovae (SNe Ia), two white dwarfs orbiting one another are gradually driven together by gravitational radiation. At late phases of the inspiral when the stars are separated by a modest multiple of their radii, they will exert mutual tidal torques tending to enforce synchronism between their rotational and orbital frequencies. These torques, which likely involve resonant excitation of inertial oscillations and internal waves (g-modes), are expected to be unequally distributed within the star, in fact concentrated toward the surface where thermal timescales are shortest, densities are least, and tidally excited waves may break nonlinearly (Fuller & Lai 2012; Burkart et al. 2013; Dall’Osso & Rossi 2014), possibly with observable consequences (Fuller & Lai 2013). When the star rotates rapidly compared to the tidal frequency, i.e., when $\Omega_{\text{spin}} \gg \Omega_{\text{orbit}} - \Omega_{\text{spin}}$, the torque is also concentrated in latitude, toward the equator (Fuller & Lai 2014). Magnetic stresses are likely needed to couple the rotation of the stellar interior to that of the surface layers. The amount of associated dissipation in the interior may depend not only on the strength of the magnetic field and of the tide, but also on the symmetry of the field. If it is essentially axisymmetric, then since plasma viscosity is likely negligible, some turbulent dissipation is probably required to transport angular momentum across the lines.

Also, the efficiency of magnetic redistribution of angular momentum may affect the degree of nonsynchronous rotation, which, even if small, determines the total dissipation associated with a given tidal torque. An upper bound to the tidal heating rate is the power required to maintain synchronous rotation, $\dot{E}_{\text{spin}} = (I_1 + I_2)\Omega\dot{\Omega}$, where Ω is the orbital angular velocity and $I_{1,2}$ are the moments of inertia of the two stars. For two $0.7 M_{\odot}$ carbon-oxygen white dwarfs driven together by gravitational radiation, $\dot{E}_{\text{spin}} \approx 10^{38} P_{\text{min}}^{-14/3} \text{ erg s}^{-1}$, where P_{min}

is the orbital period in minutes, while the time before contact is $400 P_{\text{min}}^{-8/3}$ year. As noted in the works cited above, however, the actual dissipation rate will be less than this by an appropriate average of $(1 - \Omega_{\text{spin}}/\Omega_{\text{orb}})$, Ω_{spin} being the rotational angular velocity of each mass element (which differs among elements if the star rotates differentially). Thus the dissipation will be quite small if the tidal torques are efficiently redistributed so that all parts of the star are kept nearly synchronous with the orbit. The dissipation will also be small if the tidal torques are weak so that $\dot{\Omega}_{\text{spin}} \ll \dot{\Omega}_{\text{orb}}$. Still, if even a small fraction of \dot{E}_{spin} were dissipated and the heat were transported to the surface, such systems could be quite luminous.

Surface magnetic fields of white dwarfs vary widely. Zeeman measurements indicate that $\sim 10\%$ of these stars have fields exceeding 2 MG (Liebert et al. 2003), but sensitive polarimetry (of admittedly small samples) suggests that the majority have surface fields $\lesssim 10$ kG (Landstreet et al. 2012). In the expected absence of dynamo action, electrical conductivities in the degenerate interiors of these stars are such that their fields should decay on timescales $\sim 10^9$ year (Fontaine et al. 1973). This is of the same order as the ages of most observed white dwarfs and likely also of many SNe Ia progenitors. Depending upon the star’s mass, crystallization begins at the center after one to a few billion years when the luminosity has fallen to 10^{-3} – $10^{-4} L_{\odot}$ (Renedo et al. 2010). Some field lines may be anchored to the growing solid core, an effect not accounted for in the idealized models considered here.

The double-degenerate scenario for SNe Ia, though favored by recent evidence, is unproven (Maoz et al. 2014). A variant invokes merging via head-on collisions in a triple-star system rather than inspiral driven by gravitational waves (Katz & Dong 2012; Kushnir et al. 2013). Yet short-period white-dwarf binaries do exist (Nelemans et al. 2004; Brown et al. 2011), and their end states invite speculation even if they are not destined to be supernovae.

The plan of this paper is as follows. Section 2 frames the free-decay problem and our numerical methods. Section 3 compares results for the kinematic problem, in which the differential rotation is prescribed and the backreaction of the field neglected, with the predictions of Rädler (1986). Section 4 presents results for the full nonlinear problem, including estimates for the critical initial field strength as a function of Rm . Numerical considerations limit our calculations to $Re = Rm \leq 10^4$, much less than in a real white dwarf. Finally, Section 5 discusses the relationship of these numerical results to the astrophysical problem that motivates this work. It is clear that there are many aspects of the joint tidally driven evolution of the magnetic field and differential rotation that will need further study.

2. FORMULATION

We calculate the three-dimensional and fully nonlinear unforced MHD equations in a spherical shell with inner radius r_i and outer radius r_o . The differential rotation and misaligned field are given as initial conditions. To conserve total angular momentum, stress-free conditions are imposed on the fluid velocity and insulating conditions on the magnetic field at both boundaries.

The dimensionless MHD equations for an incompressible fluid of constant and uniform density read

$$\frac{\partial \mathbf{u}}{\partial t} + \mathbf{u} \cdot \nabla \mathbf{u} = -\nabla p + \frac{1}{Re} \nabla^2 \mathbf{u} + (\nabla \times \mathbf{B}) \times \mathbf{B}, \quad (1)$$

$$\frac{\partial \mathbf{B}}{\partial t} = \nabla \times (\mathbf{u} \times \mathbf{B}) + \frac{1}{Rm} \nabla^2 \mathbf{B}. \quad (2)$$

Length has been normalized to r_o , time to Ω_0^{-1} , velocity to $\Omega_0 r_o$ where Ω_0 is characteristic of the initial angular velocity (see Equation (7)), pressure to $\rho \Omega_0^2 r_o^2$, and magnetic field to $\sqrt{\rho \mu} \Omega_0 r_o$. There are three dimensionless parameters governing the MHD flow. The Reynolds number $Re = \Omega_0 r_o^2 / \nu$, where ν is kinematic viscosity, is the ratio of the viscous timescale to the initial rotational timescale. Similarly, the magnetic Reynolds number $Rm = \Omega_0 r_o^2 / \eta$, where η is magnetic diffusivity, is the timescale for diffusion of the initial magnetic field relative to the rotation time. For numerical feasibility, we keep $Re = Rm$, namely the magnetic Prandtl number Pm is unity. The dimensionless Alfvén velocity $Va = B_0 / (\sqrt{\rho \mu} \Omega_0 r_o)$, where B_0 is characteristic of the initial field (see Equation (10)), measures the strength of initial field relative to initial rotation. To minimize the effect of the inner sphere while avoiding the coordinate singularity at the origin, we take $r_i / r_o = 0.1$.

The details of numerical method can be found in Hollerbach (2000). Toroidal–poloidal decompositions are used to guarantee $\nabla \cdot \mathbf{u} = \nabla \cdot \mathbf{B} = 0$:

$$\begin{aligned} \mathbf{u} &= \nabla \times (e \hat{\mathbf{e}}_r) + \nabla \times \nabla \times (f \hat{\mathbf{e}}_r), \\ \mathbf{B} &= \nabla \times (g \hat{\mathbf{e}}_r) + \nabla \times \nabla \times (h \hat{\mathbf{e}}_r). \end{aligned} \quad (3)$$

Note that the toroidal part $\nabla \times (e \hat{\mathbf{e}}_r)$ has a latitudinal component proportional to $\partial e / \partial \phi$, and that the poloidal part $\nabla \times \nabla \times (f \hat{\mathbf{e}}_r)$ has an azimuthal component proportional to $\partial^2 f / \partial \phi \partial r$. Therefore, when speaking of non-axisymmetric fields, we will refer to components parallel to \mathbf{e}_ϕ as *azimuthal* (rather than toroidal), and to components parallel to the r – θ plane as *meridional* (rather than poloidal), to avoid confusion caused by experience with axisymmetry, where “toroidal” is synonymous with “azimuthal,” and “poloidal” with “meridional.”

In spherical coordinates (r, θ, ϕ) the functions $\{e, f, g, h\}$ are expanded in the angular coordinates with spherical harmonics and in radius with Chebyshev polynomials. For example,

$$\begin{aligned} e(r, \theta, \phi, t) &= \sum_{l,m} [e_{lm}^c(r, t) P_l^m(\cos \theta) \cos(m\phi) \\ &\quad + e_{lm}^s(r, t) P_l^m(\cos \theta) \sin(m\phi)], \\ e_{lm}^c(r, t) &= \sum_k e_{klm}^c(t) T_k(x) \text{ and } e_{lm}^s(r, t) \\ &= \sum_k e_{klm}^s(t) T_k(x), \end{aligned} \quad (4)$$

where $x = (2r - r_o - r_i) / (r_o - r_i) \in [-1, +1]$. We use a second order Runge–Kutta scheme for time stepping. The diffusive terms are treated implicitly.

We impose a stress-free boundary condition for fluid velocity at both r_o and r_i , namely $u_r = \tau_{r\theta} = \tau_{r\phi} = 0$.

Translated to spherical harmonics, this becomes

$$f_{lm} = \frac{d}{dr} \left(\frac{1}{r^2} \frac{d f_{lm}}{dr} \right) = \frac{d}{dr} \left(\frac{1}{r^2} e_{lm} \right) = 0. \quad (5)$$

These hold for both cosine and sine components and so the superscripts c and s are omitted. We require the field to match onto potential fields interior to r_i and exterior to r_o that are regular at $r = 0$ and $r = \infty$, respectively, so that

$$\begin{aligned} g_{lm} &= \left(\frac{d}{dr} - \frac{l+1}{r} \right) h_{lm} = 0 \text{ at } r_i, \\ g_{lm} &= \left(\frac{d}{dr} + \frac{l}{r} \right) h_{lm} = 0 \text{ at } r_o. \end{aligned} \quad (6)$$

The initial differential rotation profile is taken for the hydrostatic equilibrium, i.e., inertial force is balanced by pressure gradient, such that the angular velocity depends only on cylindrical radius $R = r \sin \theta$,

$$\Omega = \Omega_0 r^2 \sin^2 \theta. \quad (7)$$

Nonmagnetic force balance with more general patterns of differential rotation would require stratification, which we wish to avoid. It seems unlikely that this simplification qualitatively affects the competition between differential rotation and non-axisymmetry, but it does restrict the allowable isorotational states in case the former triumphs over the latter. A larger exponent of R might better imitate the concentration of tidal torques toward the surface and equator but would lead to rapid magnetic and viscous diffusion at the numerically accessible values of Re and Rm . Like this profile, the differential rotation resulting from tidal torques in an inspiraling binary is probably immune to magnetorotational instability because $\partial \Omega^2 / \partial R > 0$ (e.g., Balbus 2003).

For the initial field we choose free-decay modes, eigenfunctions of the induction equation with finite conductivity and currents confined to the body (Moffatt 1978, Section 2.7). If the conductivity is uniform, the poloidal expansion coefficients obey

$$\frac{\partial h_{lm}}{\partial t} = \frac{\partial^2 h_{lm}}{\partial r^2} - \frac{l(l+1)}{r^2} h_{lm}. \quad (8)$$

The eigenfunctions for h_{lm} are linear combinations of spherical Bessel functions of the first and second kind that satisfy the insulating boundary condition (6). We choose for the initial conditions a linear combination of the two lowest-order poloidal free-decay modes ($l = 1, m = 0$) and ($l = 1, m = 1$):¹

$$h(r) = h_{10}(r) \cos \alpha + h_{11}(r) \sin \alpha, \quad (9)$$

¹ These modes suffice to match onto a general dipole field in the vacuum exterior to the star. In white dwarfs, modes with higher l and/or more radial nodes would undergo significant resistive decay on Gyr timescales.

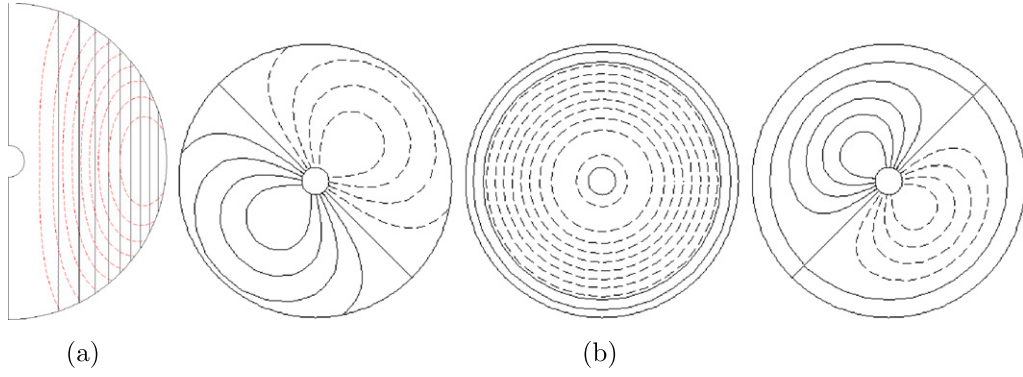


Figure 1. Initial conditions with magnetic obliquity $\alpha = 45^\circ$. (a) Contours of initial axisymmetric angular velocity (black lines) and poloidal field (red lines) in the meridional plane. (b) Contours of the components of initial field in the equatorial plane: B_r , B_θ , and B_ϕ (left to right). In both (a) and (b), solid lines denote positive and dashed negative.

in which α is the angle between the rotational and magnetic axes. The initial field is then

$$\begin{aligned}
 B_r &= B_0 \frac{2}{r^2} \left[h_{10}^c \cos \theta \cos \alpha - \sin \theta \right. \\
 &\quad \left. \times (h_{11}^c \cos \phi + h_{11}^s \sin \phi) \sin \alpha \right], \\
 B_\theta &= -B_0 \frac{1}{r} \left[\frac{dh_{10}^c}{dr} \sin \theta \cos \alpha + \cos \theta \right. \\
 &\quad \left. \times \left(\frac{dh_{11}^c}{dr} \cos \phi + \frac{dh_{11}^s}{dr} \sin \phi \right) \sin \alpha \right], \\
 B_\phi &= B_0 \frac{1}{r} \left(\frac{dh_{11}^c}{dr} \sin \phi - \frac{dh_{11}^s}{dr} \cos \phi \right) \sin \alpha. \quad (10)
 \end{aligned}$$

The normalization is chosen so that the initial magnetic energy is $Va^2 \rho \Omega_0^2 r_0^5$, where $\rho \Omega_0^2 r_0^5$ is unity in our scaled units. The initial field has a nonzero azimuthal component unless $\sin \alpha = 0$. Figure 1(a) shows the meridional distributions of initial angular velocity (black lines) and poloidal field (red lines) and Figure 1(b) shows the three components of initial field in the equatorial plane for $\alpha = 45^\circ$.

With the boundary conditions, the total angular momentum should be conserved, and with our initial conditions, it is purely axial:

$$\begin{aligned}
 L_z &= \int_V r \sin \theta u_\phi dV = \frac{4}{3} \pi (r_o - r_i) \\
 &\quad \times \sum_k e_{k10}^c \int_{-1}^{+1} r^2 T_k(x) dx. \quad (11)
 \end{aligned}$$

The radial integral can be found analytically. In our numerical calculations, e_{k10}^c is monitored at each time step, and the total angular momentum is found to be conserved to one part in 10^8 . For the initial rotation profile (7), $L_z = 0.9574$ in our units, and the initial kinetic energy $E_0 = 0.3191$. Because of viscosity, uniform (solid-body) rotation must eventually be established. The final angular velocity and kinetic energy are $\Omega_\infty = L_z/I = 0.5714$ and $E_\infty = L_z^2/2I = 0.2736$, where $I \approx 1.676$ is the moment of inertia of the fluid shell. Therefore, the excess kinetic energy available for dissipation is $E_0 - E_\infty \approx 0.0455 \approx E_0/7$. In Section 4, we compare the times required for the magnetic and excess kinetic energies to

decay to 10% of their initial values, as functions of $Rm = Re$ and Va .

3. KINEMATIC PROBLEM

Before addressing the fully nonlinear problem, we study a simplified kinematic one in which the flow is fixed in its initial form (7), and only the magnetic induction Equation (2) is solved. This is a linear problem and the spherical harmonics decouple. Therefore, the axisymmetric and non-axisymmetric fields evolve independently.

Rädler (1986)'s analysis applies here, and we summarize it. Differential rotation shears the axisymmetric meridional field into an axisymmetric azimuthal field—the so-called ω effect—with the same dependence on (r, θ) and therefore a constant characteristic decay time $t_d = r_o^2/\eta$. However, if diffusion is neglected, the non-axisymmetric field reverses on progressively finer length scales as time goes on. Rädler demonstrates this with a cartoon of a field line winding up in a plane, but the point is important enough to us that we give a more careful argument. In ideal MHD, advection by the velocity field $\Omega(r, \theta)r \sin \theta \hat{e}_\phi$ preserves the meridional components $\mathbf{B}_p \equiv (B_r, B_\theta)$ along the flow, as can be seen by considering that any closed fluid contour drawn on a sphere $r = \text{constant}$ remains on the sphere and encloses constant area and constant flux as it is advected; and similarly for any contour on a cone $\theta = \text{constant}$. Therefore, if $\mathbf{B}_p^{(t)}(r, \theta, \phi)$ is the meridional field at time t , then the evolution of this field and its derivatives is

$$\begin{aligned}
 \mathbf{B}_p^{(t)}(r, \theta, \phi) &= \mathbf{B}_p^{(0)}[r, \theta, \phi - \Omega(r, \theta)t], \\
 \frac{\partial}{\partial r} \mathbf{B}_p^{(t)}(r, \theta, \phi) &= \frac{\partial}{\partial r} \mathbf{B}_p^{(0)}[r, \theta, \phi - \Omega(r, \theta)t] \\
 &\quad + t \frac{\partial \Omega}{\partial r} \frac{\partial}{\partial \phi} \mathbf{B}_p^{(0)}[r, \theta, \phi - \Omega(r, \theta)t], \\
 \frac{\partial}{\partial \theta} \mathbf{B}_p^{(t)}(r, \theta, \phi) &= \frac{\partial}{\partial \theta} \mathbf{B}_p^{(0)}[r, \theta, \phi - \Omega(r, \theta)t] \\
 &\quad + t \frac{\partial \Omega}{\partial \theta} \frac{\partial}{\partial \phi} \mathbf{B}_p^{(0)}[r, \theta, \phi - \Omega(r, \theta)t],
 \end{aligned}$$

from which it can be seen that the meridional derivatives $\partial_r \mathbf{B}_p$ and $\partial_\theta \mathbf{B}_p$ increase linearly with time unless $\partial \mathbf{B}_p^{(0)}/\partial \phi = 0$ (axisymmetry) or $\nabla \Omega = 0$ (solid-body rotation). Yet the first line above implies that $\int |\mathbf{B}_p^{(t)}|^2 dV$ is constant. Therefore, the

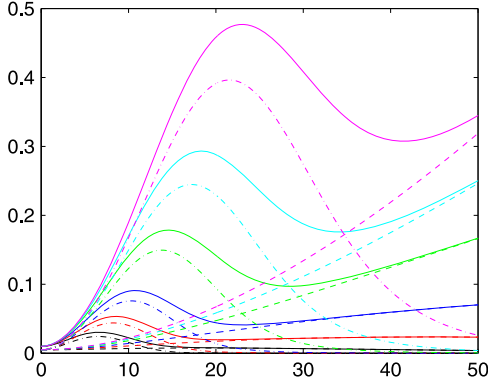


Figure 2. Time evolution of total (solid), axisymmetric (dashed), and non-axisymmetric (dash-dot) magnetic energy in the kinematic problem at $Va = 0.1$ and $\alpha = 45^\circ$. Curves from bottom to top (colored black, red, blue, green, cyan, and magenta) denote respectively $Rm = 500, 1000, 2000, 5000, 10,000$ and $20,000$.

non-axisymmetric part of $B_p^{(t)}$ must reverse direction on progressively smaller scales, as was to be shown. Finally, since the meridional field is the source of the growing azimuthal field via the term $\propto B_p \cdot \nabla \Omega$ in the induction equation, the non-axisymmetric part of $B_\phi^{(t)}$ must also develop such reversals.

Given a small diffusivity η , it follows that the resistive timescale of the m th azimuthal harmonic decreases as $t_{d,m} \sim \eta^{-1} m^{-2} |\nabla \Omega|^{-2} t^{-2}$ at late times ($m \neq 0$) where the length scale is taken to be $(m |\nabla \Omega| t)^{-1}$, i.e., the length scale of shear $(|\nabla \Omega| t)^{-1}$ divided by number of polarity reversals m . Once $t_{d,m} \lesssim t$, all components of the m th harmonic quickly decay. Thus the toroidal field and magnetic energy will peak at a time

$$t_{\text{peak}} \sim \begin{cases} (m^{-2} \eta^{-1} |\nabla \Omega|^{-2})^{1/3} \equiv m^{-2/3} (Rm')^{1/3} (\Delta \Omega)^{-1} & m \neq 0, \\ Rm' (\Delta \Omega)^{-1} & m = 0, \end{cases} \quad (12)$$

where $\Delta \Omega \sim r_0 |\nabla \Omega|_{\text{rms}}$ is a measure of the differential rotation, and $Rm' \equiv r_0^2 \Delta \Omega / \eta$. The peak magnetic energy density therefore scales as

$$E_{\text{mag,peak}} \sim \begin{cases} (Rm')^{2/3} E_{\text{mag,init}} m^{-4/3} & m \neq 0, \\ (Rm')^2 E_{\text{mag,init}} & m = 0, \end{cases} \quad (13)$$

unless the $m = 0$ component of the field is isorotational.

Figure 2 shows the time evolution of total, axisymmetric, and non-axisymmetric magnetic energy at different Rm with $Va = 0.1$ and $\alpha = 45^\circ$. Initially, the axisymmetric azimuthal magnetic field grows linearly with time and its energy grows quadratically, but eventually all components of the field decay resistively. The non-axisymmetric energy grows faster and decays much faster than the axisymmetric energy. The peak value of non-axisymmetric magnetic energy and the time at which it is achieved are given in Table 1. These results can be fit by $t_{\text{peak}} \propto Rm^{0.323 \pm 0.004}$ and $E_{\text{mag,peak}} \propto Rm^{0.753 \pm 0.035}$, in rough agreement with Equations (12) and (13). The exponent of the latter fit is influenced by behavior at small Rm ; between the two *highest-Rm* points, the logarithmic slope is 0.696. A

toy model that we will not go into here suggests that both exponents can be expected to differ from their asymptotic values as $Rm \rightarrow \infty$ by corrections of relative size $\sim Rm^{-1/3}$. This explains the deviations of $E_{\text{mag,peak}}$ from its expected asymptotic scaling rather well, leaving as a mystery why the t_{peak} scaling does not deviate more than observed.

4. SELF-CONSISTENT MHD FLOW

We now study the fully nonlinear MHD flow by numerically solving both (1) and (2). The importance of the magnetic forces can be estimated by comparing the peak magnetic energy (13) predicted kinematically to the energy available in the shear flow: this ratio is $\sim Va^2 Rm^{2/3}$ for $m = 1$. Thus, if $Va \gtrsim Rm^{-1/3}$, the non-axisymmetric field can be expected to act as a brake on the large-scale shear before it is annihilated by diffusion (Spruit 1999). For $Re^{-1} \ll Va \ll Rm^{-1/3}$, the field will be symmetrized but will eventually drive the flow toward isorotation (in the sense of Ferraro's law) before viscosity enforces solid-body rotation. Finally, if $Va \ll Re^{-1}$, the kinematic approximation should describe the flow reasonably well at all times. All this presumes that the axisymmetric and non-axisymmetric field strengths are initially comparable. The effect of varying the misalignment angle α is described at the end of this section. Unfortunately, numerical considerations dictate that we adopt $Re = Rm$ rather than $Re \gg Rm$, so we must use some care to distinguish magnetic from viscous effects.

The influence of the non-axisymmetric field can also be described as a form of phase mixing, but one that involves azimuthal advection by the velocity field as well as Alfvénic propagation along the lines. As in the axisymmetric case, fluid elements on the same field line can exchange angular momentum through magnetic tension, and differing rates of propagation on neighboring lines leads to phase mixing and damping of the associated Alfvén waves. But since the field is non-axisymmetric, the projections of magnetic field lines onto the meridional may intersect. Insofar as the velocity field remains approximately axisymmetric and predominantly rotational, the differential rotation may bring points on two such lines arbitrarily close together, even though these points are initially widely separated in azimuth. The combination of these Alfvénic and advective processes may drive the entire volume to a uniform angular velocity, provided that the non-axisymmetric field persists.

First we study the magnetic backreaction by varying the initial field strength. Figure 3 compares the time evolution of magnetic energy in the kinematic problem with that of the self-consistent MHD flow at different Va . Evidently, the latter approaches the kinematic behavior at low Va . In the first panel, the magnetic field is so strong ($Va = 0.1 > Rm^{-1/3} \approx 0.06$) that it modifies the rotation profile significantly, as can be seen in Figure 4(a). The peak magnetic energy of the self-consistent solutions is limited by the excess kinetic energy available in the initial differential rotation ($\Delta E_0 \approx 0.0455$, Section 2).

Figure 4 shows the flow and field for the same simulation as in the first panel of Figure 3 at the time when the non-axisymmetric magnetic energy peaks, $t = 7.48$. The first panel shows a large change in the pattern of differential rotation compared to the initial state (Figure 1(a)). Meridional circulation is induced, as shown in the right panel. The winding-up of the field is evident in the plan views shown in the last three panels.

Table 1
Time to Reach the Peak of Non-axisymmetric Magnetic Energy and the Peak Value of that Energy for the Kinematic Calculations in Figure 2

Rm	500	1000	2000	5000	10000	20000
t_{peak}	6.5	8.2	10.3	13.8	17.2	21.5
$E_{\text{mag,peak}}$	2.431×10^{-2}	4.396×10^{-2}	7.591×10^{-2}	1.495×10^{-1}	2.447×10^{-1}	3.963×10^{-1}

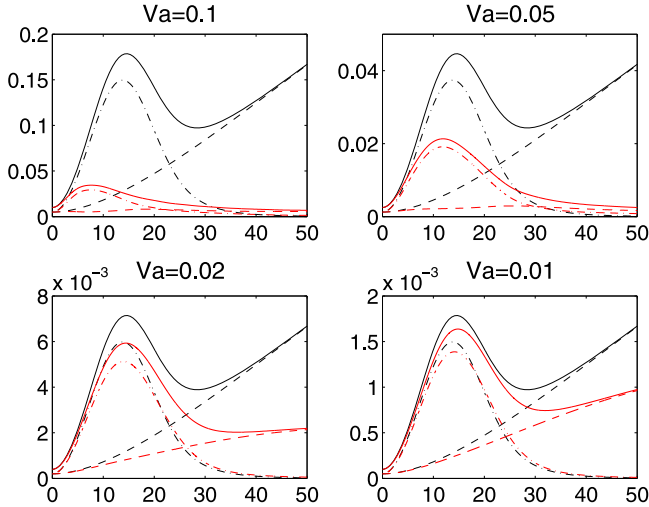


Figure 3. Time evolution of total (solid), axisymmetric (dashed) and non-axisymmetric (dash-dot) magnetic energy in both the kinematic problem (black) and self-consistent flow (red). $Re = Rm = 5000$ and $\alpha = 45^\circ$.

Next we discuss the applicability of the isorotation law $\mathbf{B}_p \cdot \nabla \Omega = 0$. The non-axisymmetric field alters the conditions for isorotation. Suppose that $\mathbf{u} = R\Omega \hat{e}_\phi$ and $\mathbf{B} = B_R \hat{e}_R + B_z \hat{e}_z$ in cylindrical coordinates (R, ϕ, z) , and that $Rm \rightarrow \infty$ so that magnetic diffusion is ineffective. In axisymmetry, the induction term $\nabla \times (\mathbf{u} \times \mathbf{B}) = R(\mathbf{B}_p \cdot \nabla \Omega) \hat{e}_\phi$. If this vanishes, then $\partial \mathbf{B} / \partial t = 0$, so that isorotation can be maintained indefinitely, with different angular velocities on different magnetic surfaces (surfaces parallel to the field lines). When the field depends nontrivially on the azimuthal coordinate (ϕ) , however, the induction term becomes

$$\nabla \times (\mathbf{u} \times \mathbf{B}) = R(\mathbf{B}_p \cdot \nabla \Omega) \hat{e}_\phi - \Omega \left(\frac{\partial B_R}{\partial \phi} \hat{e}_R + \frac{\partial B_z}{\partial \phi} \hat{e}_z \right).$$

Even if $\mathbf{B}_p \cdot \nabla \Omega$ is initially zero, the second term on the right side will cause \mathbf{B}_p to evolve, so that additional constraints must be satisfied by the initial state to maintain isorotation. It is likely that there are very few if any non-axisymmetric isorotational states other than solid-body rotation (Mestel & Weiss 1987). Since the non-axisymmetric field decays much faster than the axisymmetric field, however, it may be that isorotation can be approached on intermediate timescales when the field is substantially axisymmetric but viscosity has not yet eliminated all shear in the velocities. Such intermediate states are possible in the regime $Re^{-1} \ll Va \ll Rm^{-1/3}$. Figure 5 shows the contours of axisymmetric angular velocity and poloidal field lines at $Va = 0.1$ and 0.01 : the former is outside the regime in question, while the latter is within it. In each subfigure the four panels are taken at intermediate times after the peak of the non-axisymmetric magnetic energy (see upper-

left and bottom-right panels in Figure 3) but much earlier than $\Omega^{-1} Re$. Figure 5(a) suggests that the isorotational state is destroyed by the stronger field, while Figure 5(b) suggests that it is nearly achieved for the weaker field in the deeper interior. In the latter case, the angular velocity is nearly a function of cylindrical radius alone, as required for steady unstratified flow when magnetic and other non-potential forces are unimportant. (Some dependence on z as well as R might have resulted if we had allowed for stratification.) The magnetic field lines are approximately parallel to the rotation axis at depth but not near the surface. They resemble the shape of the slowest-decaying resistive magnetic eigenfunction in a uniformly rotating and uniformly conducting shell, especially near the equator (Figure 1(a)).

Thirdly we compare the relative strength of differential rotation and misaligned field. As pointed out by Mestel (1999, Section 9.3), the degree of misalignment is crucial to the dynamics. To quantify the relative strength we compare two characteristic times. The first is the time when the excess kinetic energy drops to 10% of its initial value. As noted in Section 2, the kinetic energy decays from 0.3191 initially to 0.2736 in a state of uniform rotation at the same total angular momentum; thus the reduction of the difference of these by 90% corresponds to kinetic energy = 0.2781. The second characteristic time is that when the non-axisymmetric magnetic energy drops to 10% of its peak (not initial) value. Table 2 lists these two times for several $Re = Rm$ and Va . In each column higher Va corresponds to faster decay of kinetic energy and slower decay of non-axisymmetric magnetic energy. A stronger field tends to convert more kinetic energy to magnetic energy, as already seen in Figure 3 and the surrounding discussion above. More importantly, in the regime $Va \leq 0.03$ the time for the 90% drop of kinetic energy is later than the time for the 90% drop of non-axisymmetric magnetic energy, whereas in the regime $Va \geq 0.05$ the situation is reversed. Therefore, there exists a boundary in the (Rm, Va) plane across which the dynamics is qualitatively changed. Below this boundary the magnetic field is symmetrized before differential rotation completely decays; above it, differential rotation is suppressed before the magnetic field is symmetrized (if it is symmetrized at all before it decays). This is consistent with the arguments of Mestel (1999) and Spruit (1999).

To test these arguments more quantitatively, we have interpolated in Va along each column of Table 2 to find the value Va_{crit} at which the two times in question are equal. The bottom row of Table 2 indicates that Va_{crit} is not a monotonic function of Rm . A power-law fit to the final two columns (the highest Rm) yields $Va_{\text{crit}} \propto Rm^{-0.20}$, a somewhat weaker dependence than the scaling $Rm^{-1/3}$ predicted by the quasi-kinematic reasoning at the beginning of this section. We return to this point in Section 5 below.

To end this section, we briefly discuss the effect of varying the angle α between the rotational and magnetic axes. Since, as we have seen, there are strong differences between the

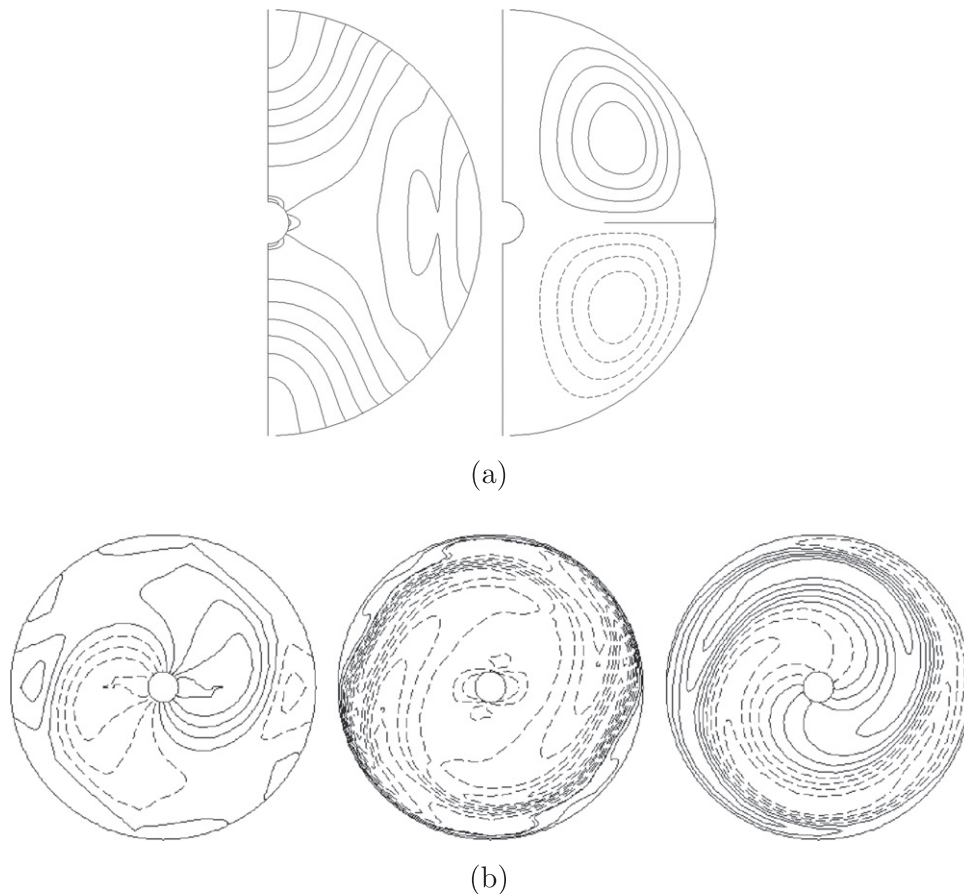


Figure 4. Sequel to Figure 1 at the time when the non-axisymmetric magnetic energy peaks ($t = 7.48$); $Re = Rm = 5000$, $Va = 0.1$ and $\alpha = 45^\circ$. (a) Contours of axisymmetric angular velocity (left panel) and meridional circulation (right panel) in the meridional plane. (b) Contours of B_r , B_θ , and B_ϕ in the equatorial plane. In both (a) and (b), solid lines denote positive and dashed negative.

axisymmetric cases (where $\alpha = 0$) and those for which $\alpha = 45^\circ$, it is reasonable to expect that the strength of the interaction between the flow and the field should increase continuously with this angle up to $\alpha = 90^\circ$. This expectation is tested in Figure 6, which shows the evolution of the magnetic energy and Ohmic dissipation for several values of α . A larger angle leads to higher energy and dissipation, as expected. In fact, for the cases shown in Figure 6 and tabulated in Table 3, the peak of the non-axisymmetric energy increases linearly with $\sin^2 \alpha$ (correlation coefficient 0.9999). This would not be surprising in the kinematic problem, since the initial amplitude of the non-axisymmetric component is proportional to $\sin \alpha$, but the calculations shown in Figure 6 include magnetic backreaction. Of course the energy $E_{\text{mag,peak}}$ (and somewhat more, because dissipation has already begun to act at the time of the peak) must come at the expense of the differential rotation.

5. DISCUSSION

In this work we have explored numerically the interaction of differential rotation and a misaligned magnetic field. In the kinematic limit we verify the $Rm^{1/3}$ law for the time and amplitude at which the non-axisymmetric azimuthal field reaches its peak and then decays, whereas the corresponding scaling for the axisymmetric field is $O(Rm)$. In self-consistent calculations where the flow reacts to magnetic forces, a sufficiently weak magnetic field behaves approximately as in

the kinematic problem, becoming axisymmetric before the rotation becomes uniform, and a nontrivial state of isorotation—one in which different magnetic surfaces have different angular velocities—is approximately achieved near the rotation axis. For stronger fields, there exists a boundary in the plane of dimensionless initial magnetic field strength Va versus Rm above which differential rotation is suppressed before the non-axisymmetric magnetic field decays. This boundary is better described by $Va_{\text{crit}} \propto Rm^{-0.20}$ than by the expected scaling $Rm^{-1/3}$, at least over the range explored by our simulations ($Rm \leq 10^4$). We do not understand this quantitatively for our actual simulations, though according to the arguments given below, one expects the dependence of Va_{crit} on Rm to weaken at very large Rm because of reconnection and perhaps other nonlinear processes that assist in the destruction of the non-axisymmetric field. We have also verified that a larger misalignment angle (α) between the rotational and magnetic axes leads to stronger exchanges between the flow and the field, in proportion to $\sin^2 \alpha$ (Figure 6).

In our calculations the magnetic Prandtl number $Pm \equiv Rm/Re = \nu/\eta$ has been fixed at unity for numerical convenience. With the code and computational resources available to us, fully resolved simulations are practical only if the larger of Re and Rm is $\lesssim 10^4$. Therefore, we approach ideal MHD best by taking $Re = Rm$. Direct numerical simulations of magnetic dynamos (e.g., Schekochihin et al. 2007) and magnetorotational turbulence (e.g., Fromang et al. 2007) often

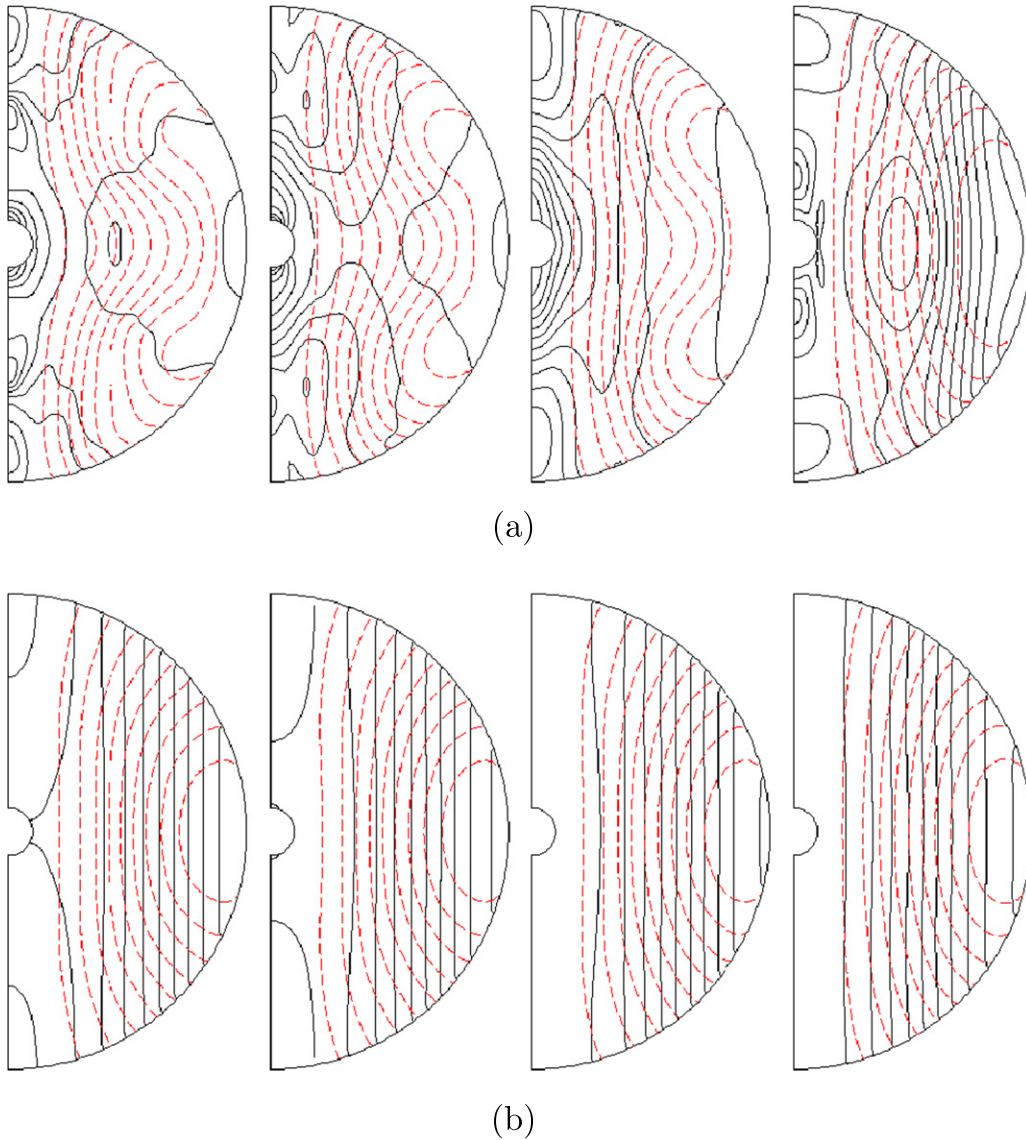


Figure 5. Contours of axisymmetric angular velocity (black lines) and magnetic field (red lines) in the meridional plane. $Re = Rm = 5000$ and $\alpha = 45^\circ$. (a) $Va = 0.1$, (b) $Va = 0.01$. In both (a) and (b) the four panels from left to right are at time = 30, 40, 50, and 100.

Table 2
Times for 90% Drop in Energy

Va	$Re = Rm$				
	500	1000	2000	5000	10,000
0.01	20.6/17.9	39.5/20.2	75.0/23.9	159.4/31.1	258.8/38.2
0.02	19.8/18.1	36.5/20.5	64.1/24.2	115.6/31.6	185.9/38.9
0.03	18.4/18.4	32.0/21.0	50.7/25.1	72.5/32.3	60.4/38.7
0.04	16.5/18.9	26.3/21.7	35.3/26.0	34.2/32.7	30.2/45.0
0.05	14.4/19.5	20.0/22.9	21.8/27.0	23.9/33.4	25.4/47.0
0.1	8.5/21.3	9.8/26.2	11.8/31.0	19.3/37.0	...
...	0.0300	0.0461	0.0464	0.0414	0.0359

Note. The figure to the left of the slash is the time when the kinetic energy drops 90% of its initial value and the figure to the right is the time when the non-axisymmetric magnetic energy drops 90% of its peak value. The bottom row is Va_{crit} . The calculation is done for five values of $Re = Rm$: that at $Re = Rm = 10,000$ and $Va = 0.1$ was incompletely resolved.

find that Pm influences large-scale properties of the flow, at least within the computationally accessible range of Re and Rm . Whether Pm remains macroscopically important at much larger

Rm and Re , as in real stars and in the interstellar medium, can only be addressed at present via idealized models of turbulence (Kulsrud & Anderson 1992; Malyskin & Boldyrev 2009; Schober et al. 2012). It is worth noting, however, that in comparison to Re and Rm themselves, Pm is not so far from unity in the applications of interest to us. At $r = 0.5 R_\odot$ in the Sun (where $T \approx 4 \times 10^6$ K and $\rho \approx 1.3$ g cm $^{-3}$), one estimates from the classical Spitzer formulae that $Pm \approx 10^{-2}$. For white-dwarf interiors at $T \sim 10^6$ – 10^7 K and $\rho \sim 10^6$ g cm $^{-3}$, we estimate² $Pm \sim 10^2$ – 10^3 .

Another simplification we have made is to neglect stratification, an important effect in the outer parts of white dwarfs, where there are significant entropy and composition gradients, and in the radiative zone of the Sun. As noted in Section 1, stratification

² Using the results of Yakovlev & Urpin (1980) as encoded in the FORTRAN programs at www.ioffe.ru/astro/conduct, which return electrical and thermal conductivities. We roughly translate the latter to a kinematic viscosity by multiplying by $m_i/k_b\rho$, m_i being the ion mass, presuming that the material has not crystallized.

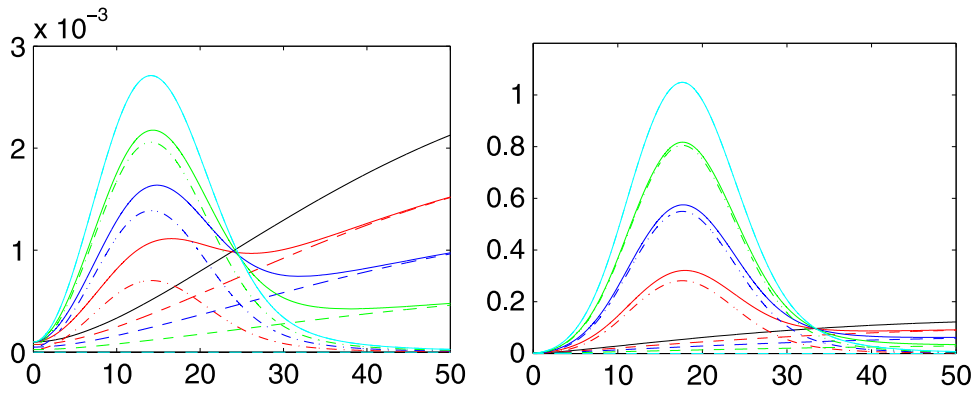


Figure 6. Time evolution of magnetic energy (left panel) and Ohmic dissipation (right panel) at different magnetic obliquities. $Re = Rm = 5000$ and $Va = 0.01$. Black, red, blue, green, and cyan lines denote respectively $\alpha = 0^\circ, 30^\circ, 45^\circ, 60^\circ,$ and 90° . Solid, dashed, and dash-dot lines denote respectively the total, axisymmetric, and non-axisymmetric energy or dissipation ($\alpha = 0^\circ$ and $\alpha = 90^\circ$ are entirely axisymmetric and non-axisymmetric, respectively).

Table 3
Peak Non-axisymmetric Magnetic Energy vs. Magnetic Obliquity α , Following Figure 6

α	0°	30°	45°	60°	90°
$E_{\text{mag,peak}}$	0	7.019×10^{-4}	1.387×10^{-3}	2.057×10^{-3}	2.711×10^{-3}

Note. $Re = Rm = 5000$ and $Va = 0.01$.

would allow a larger range of isorotational final states in hydrostatic equilibrium. The ratio of Brunt–Väsälä frequency to rotation frequency (N/Ω) is important for the growth rates of magnetic instabilities that may gradually modify the differential rotation as well as the field itself (Spruit 1999). However, we do not expect that stratification has a major effect on the interaction between a non-axisymmetric field and differential rotation (e.g., the dependence of Va_{crit} on Rm), at least on the dynamical timescales simulated here. Nor have we allowed for compressibility or density gradients. All of these could be the subject of future work, perhaps based on realistic models of representative stellar models.

Notwithstanding these caveats, we tentatively suggest some implications for real stars. As discussed in Section 1, this work has been motivated in part by tidal interactions between white dwarfs in binary orbits decaying under the influence of gravitational radiation. The calculations we have performed, however, are not directly applicable to that astrophysical problem. For one thing, the magnetic Reynolds number of a white dwarf is enormous: $Rm \sim 10^{17}$ for diffusivity $\eta \approx 1 \text{ cm}^2 \text{ s}^{-1}$ (Yakovlev & Urpin 1980), radius $R \approx 0.01 R_\odot \approx 7 \times 10^8 \text{ cm}$, and angular velocity $\Omega = 2\pi/1\text{minute}$. Solar flares and other more theoretical evidence suggest that under such nearly ideal conditions, the destruction of magnetic energy proceeds more rapidly than by linear resistive diffusion. It is plausible that nonlinear dissipative processes are already important at the modest values of Re and $Rm \sim 10^3$ in our simulations. This may account for the difference between the predicted and observed scalings of Va_{crit} with Rm . While a variety of collisionless-plasma effects have been invoked to explain the observed rate of magnetic energy release in solar flares, recent theoretical work indicates that even in classical resistive MHD, oppositely directed field lines may approach one another and annihilate at a speed $V_{\text{rec}} \approx fV_A$ that is independent of the true microscopic diffusivity (η), provided that the Lundquist number $S \equiv LV_A/\eta \gtrsim 10^4$, where V_A is the physical Alfvén speed

and L is an appropriate macroscopic length scale, such as the length of the reconnecting current sheet; the present estimate for the dimensionless factor is $f \approx 0.02$ (Loureiro et al. 2012, and references therein). Mechanisms by which V_{rec}/V_A becomes independent of η (or perhaps depends upon it only very weakly) are said to provide “fast reconnection.”

In our problem, V_A should be based on the tightly wound azimuthal field, which scales with time t as $V_A \sim Va R\Omega\Delta\Omega t$ as explained in Section 3, while the length scale along field lines is $L \sim r_0$. Thus $S \sim Va Rm'$. The local timescale on which the field is destroyed now becomes l/V_{rec} rather than l^2/η , with $l \sim r_0/(t\Delta\Omega)$ being the cross-field length scale on which the field reverses. Equating this local timescale to the winding time t leads to a revised estimate of the time at which the magnetic energy should reach its peak: $\Delta\Omega t_{\text{pk}} \sim (fVa\Omega/\Delta\Omega)^{-1/3}$ rather than $Rm^{-1/3}$ as before. Defining Va_{crit} so that the magnetic energy at the peak is equal to the excess kinetic energy ΔE in the initial differential rotation leads to $Va_{\text{crit}} \sim (\Omega/f\Delta\Omega)^{1/2}(\Delta E/5E_\infty)^2$, where $E_\infty = L_z^2/2I$ is the final rotational energy, and the factor 1/5 arises from $I/Mr_0^2 \approx 2/5$ as for a full sphere of mass M and constant density. Finally, setting $f \approx 0.02$, $\Delta\Omega/\Omega \approx 1$, and $\Delta E/E_\infty \approx 1/6$ yields $Va_{\text{crit}} \approx 0.011$. In short, if we were able to extend our calculations to $Re = Rm \rightarrow \infty$ with the same initial rotation profile and magnetic geometry, then we would expect Va_{crit} to tend asymptotically to $\sim 10^{-2}$ because of fast reconnection. It is unlikely that our simulations achieve fast reconnection, however, because the Lundquist number at the peak is

$$S_{\text{pk}} \sim Rm \left(\frac{Va^2 \Delta\Omega}{f\Omega} \right)^{1/3} \sim 0.4 Rm$$

where we have put $Va = 0.04$ and $\Delta\Omega/\Omega = 1$ in the final estimate. Thus our largest- Rm simulations probably undergo stable Sweet–Parker reconnection, for which $V_{\text{rec}} \propto V_A^{1/2}$ and an argument along the lines above predicts $Va_{\text{crit}} \propto Rm^{-1/4}$. In

astrophysical applications where $S \gg 10^4$, it is likely that fast reconnection dominates so that Va_{crit} becomes independent of Rm .

In an effort to cast doubt on contemporary helioseismological evidence for differential rotation in the solar core, Mestel & Weiss (1987) estimated that a meridional field $B_p > 0.03\text{G}$ would be sufficient to establish and maintain isorotation in the radiative zone. They admitted that isorotation does not require uniform rotation but went on to speculate that the latter would result if the magnetic field were “even slightly non-axisymmetric.” We are perhaps in a position to quantify this. From the results of Figure 6 and surrounding discussion, Mestel and Weiss’s estimate (of conditions sufficient to establish uniform rotation) can be sharpened to $B_p \sin \alpha > 0.03\text{G}$, where α is the magnetic obliquity. But this presumes that the differential rotation does not symmetrize the field (reduce α to zero) before solid-body rotation is established. If the field in the core is frequently regenerated by a dynamo process, we know of no way to constrain its obliquity. But if it is a fossil field established in the early history of the Sun, then the free-decay problem we have studied may apply. The magnetic Reynolds number of the radiative zone is $Rm_{\odot} \equiv R_c^2 \Omega_{\odot} / \eta \sim 10^{14}$, where we take $R_c \approx 0.7 R_{\odot}$ for the outer radius of this zone and evaluate η for $T = 4 \times 10^6\text{K}$ and $\rho = 1.3\text{g cm}^{-3}$ (i.e., conditions at $0.5 R_{\odot}$). If $Va_{\text{crit}} = Rm^{-1/3}$, then to avoid symmetrization, the field and obliquity would have to satisfy $B_p \gtrsim 10\text{G}$, considerably stronger than the estimate above but still quite modest. However, the Lundquist number $R_c \Omega_{\odot} / \eta$ of the radiative zone is on the order of $10^8 (B/1\text{G})$, so according to the discussion above, we expect to be in the regime of fast reconnection where Va_{crit} becomes independent of Rm . Adjusting the moment of inertia in the argument above for the actual density profile of the solar core (Bahcall et al. 1995), we estimate $Va_{\text{crit}} \approx 0.004$, which corresponds to $B_p \sin \alpha \approx 2\text{kG}$. It is still debated whether a fossil magnetic field in the solar radiative core can enforce solid-body rotation, however. A crucial issue is whether such a field can remain closed within the core, because if it were to connect to the convection zone, then by Ferraro’s Law the core also should rotate differentially (Gough & McIntyre 1998; MacGregor & Charbonneau 1999; Brun & Zahn 2006; Garaud & Garaud 2008; Acevedo-Arreguin et al. 2013).

A second difference between our simulations and the binary-white-dwarf problem is that we have studied the free decay of a pre-existing profile of differential rotation rather than gradual acceleration by a tidal torque. (This allowed the outcome to be discerned with less CPU time.) In the tidal-binary scenario, the system starts with an orbital period of a few hours, which is short enough to lead to merging of a pair of $0.7 M_{\odot}$ white dwarfs within 10^9 year (Section 1). Assuming that the tidal torque is absorbed in the outer layers of the star, the magnetic stress necessary to maintain synchronous rotation of the interior is

$$B_r B_{\phi} \sim \frac{I}{R^3} \frac{d\Omega}{dt} \sim 1 \left(\frac{P}{1 \text{ minute}} \right)^{-11/3} \text{MG}^2,$$

in which $I \approx 0.2MR^2$ is the moment of inertia of a cool white-dwarf model at this mass. Thus for example, if the meridional field is $\sim 10\text{kG}$, a plausible upper limit for most white dwarfs, then only a slight bending of the lines is needed to maintain

synchronism when the period is an hour or more. When the period is about a minute, however, $B_{\phi} \sim 10^4 B_r \sim 100\text{MG}$ would be required since differential rotation alone will not increase B_r . While this is not outside the range of surface fields observed in some white dwarfs, a non-axisymmetric field so tightly wound would have a resistive time $\sim 10^{-8}$ times smaller than that of the most slowly decaying magnetic eigenmode ($\sim 3 \times 10^9$ year); and magnetic reconnection would probably act on even shorter timescales, as discussed above. Hence an axisymmetric field might be expected, unless perhaps dissipation in the interior leads to non-axisymmetric turbulence that produces a magnetic dynamo. In fact, as Spruit (2002) has emphasized, a predominantly azimuthal axisymmetric field should be subject to non-axisymmetric Tayler instabilities, though in strongly stably stratified regions these instabilities will be concentrated toward the poles, whereas it is near the equator that meridional field is most needed to transmit tidal torques. Also, while some numerical evidence for such a dynamo has been claimed by Braithwaite (2006), it is still debated whether there exists dynamo action in stably stratified zones (e.g., Zahn et al. 2007). If it exists, such a dynamo might maintain B_r in a constant ratio to B_{ϕ} , allowing a lower overall stress for the same torque. By our estimates, a radial field of order 1MG would also begin to have a significant effect on the dispersion relation of g-modes at the compositional interface where they are tidally excited in the models of Fuller & Lai (2012).

In summary, while there is little doubt that the interactions among tidal torques, differential rotation, and magnetic fields are important for coalescing white-dwarf binaries, we are far from being able to predict the tidal heating and luminosity of such systems in the last stages of inspiral.

We thank Prof. Rainer Hollerbach for help with the calculation of energy and dissipation in his spectral code, and an anonymous referee for questions and criticism that materially improved the presentation. J. G. thanks the Australian National University and Mt. Stromlo observatory for their hospitality while our paper was being revised. This work was supported by the National Science Foundations Center for Magnetic Self-Organization under grant PHY-0821899.

REFERENCES

- Acevedo-Arreguin, L. A., Garaud, P., & Wood, T. S. 2013, *MNRAS*, **434**, 720
 Bahcall, J. N., Pinsonneault, M. H., & Wasserburg, G. J. 1995, *RvMP*, **67**, 781
 Balbus, S. A. 2003, *ARA&A*, **41**, 555
 Berger, L., Koester, D., Napiwotzki, R., Reid, I. N., & Zuckerman, B. 2005, *A&A*, **444**, 565
 Braithwaite, J. 2006, *A&A*, **449**, 451
 Brown, W. R., Kilic, M., Hermes, J. J., et al. 2011, *ApJL*, **737**, L23
 Brun, A. S., & Zahn, J.-P. 2006, *A&A*, **457**, 665
 Burkart, J., Quataert, E., Arras, P., & Weinberg, N. N. 2013, *MNRAS*, **433**, 332
 Cantiello, M., Mankovich, C., Bildsten, L., Christensen-Dalsgaard, J., & Paxton, B. 2014, *ApJ*, **788**, 93
 Chaplin, W. J., Christensen-Dalsgaard, J., Elsworth, Y., et al. 1999, *MNRAS*, **308**, 405
 Charbonneau, P., & MacGregor, K. B. 1992, *ApJ*, **387**, 639
 Charpinet, S., Fontaine, G., & Brassard, P. 2009, *Natur*, **461**, 501
 Córscico, A. H., Althaus, L. G., Kawaler, S. D., et al. 2011, *MNRAS*, **418**, 2519
 Cowling, T. G. 1957, *Magnetohydrodynamics* (New York: Interscience)
 Dall’Osso, S., & Rossi, E. M. 2014, *MNRAS*, **443**, 1057

- Deheuvels, S., Doğan, G., Goupil, M. J., et al. 2014, *A&A*, **564**, A27
- Deheuvels, S., García, R. A., Chaplin, W. J., et al. 2012, *ApJ*, **756**, 19
- Eggenberger, P., Montalbán, J., & Miglio, A. 2012, *A&A*, **544**, L4
- Ferraro, V. C. A. 1937, *MNRAS*, **97**, 458
- Fontaine, G., Thomas, J. H., & van Horn, H. M. 1973, *ApJ*, **184**, 911
- Fromang, S., Papaloizou, J., Lesur, G., & Heinemann, T. 2007, *A&A*, **476**, 1123
- Fuller, J., & Lai, D. 2012, *MNRAS*, **421**, 426
- Fuller, J., & Lai, D. 2013, *MNRAS*, **430**, 274
- Fuller, J., & Lai, D. 2014, *MNRAS*, **444**, 3488
- Garaud, P., & Garaud, J.-D. 2008, *MNRAS*, **391**, 1239
- Gough, D. O., & McIntyre, M. E. 1998, *Natur*, **394**, 755
- Heyvaerts, J., & Priest, E. R. 1983, *A&A*, **117**, 220
- Hollerbach, R. 2000, *IJNMF*, **32**, 773
- Ionson, J. A. 1978, *ApJ*, **226**, 650
- Katz, B., & Dong, S. 2012, arXiv:1211.4584
- Kawaler, S. D. 2014, arXiv:1410.6934
- Kulsrud, R. M., & Anderson, S. W. 1992, *ApJ*, **396**, 606
- Kushnir, D., Katz, B., Dong, S., Livne, E., & Fernández, R. 2013, *ApJL*, **778**, L37
- Landstreet, J. D., Bagnulo, S., Valyavin, G. G., et al. 2012, *A&A*, **545**, A30
- Liebert, J., Bergeron, P., & Holberg, J. B. 2003, *AJ*, **125**, 348
- Loureiro, N. F., Samtaney, R., Schekochihin, A. A., & Uzdensky, D. A. 2012, *PhPl*, **19**, 042303
- MacGregor, K. B., & Charbonneau, P. 1999, *ApJ*, **519**, 911
- Maeder, A., & Meynet, G. 2014, *ApJ*, **793**, 123
- Malyshkin, L., & Boldyrev, S. 2009, *ApJ*, **697**, 1433
- Maoz, D., Mannucci, F., & Nelemans, G. 2014, *ARA&A*, **52**, 107
- Mestel, L. 1999, *Stellar Magnetism* (Oxford: Clarendon)
- Mestel, L., & Weiss, N. O. 1987, *MNRAS*, **226**, 123
- Moffatt, H. K. 1978, *Magnetic Field Generation in Electrically Conducting Fluids* (Cambridge: Cambridge Univ. Press)
- Mosser, B., Goupil, M. J., Belkacem, K., et al. 2012, *A&A*, **548**, A10
- Nelemans, G., Yungelson, L. R., & Portegies Zwart, S. F. 2004, *MNRAS*, **349**, 181
- Rädler, K.-H. 1986, in *ESA Proc. Joint Varenna-Abastumani International School and Workshop on Plasma Astrophysics, On the effect of differential rotation on axisymmetric magnetic fields of cosmological bodies*, 569
- Renedo, I., Althaus, L. G., Miller Bertolami, M. M., et al. 2010, *ApJ*, **717**, 183
- Schekochihin, A. A., Iskakov, A. B., Cowley, S. C., et al. 2007, *NJPh*, **9**, 300
- Schober, J., Schleicher, D., Federrath, C., Klessen, R., & Banerjee, R. 2012, *PhRvE*, **85**, 026303
- Schou, J., Antia, H. M., Basu, S., et al. 1998, *ApJ*, **505**, 390
- Spruit, H. C. 1999, *A&A*, **349**, 189
- Spruit, H. C. 2002, *A&A*, **381**, 923
- Yakovlev, D. G., & Urpin, V. A. 1980, *SvA*, **24**, 303
- Zahn, J.-P., Brun, A. S., & Mathis, S. 2007, *A&A*, **474**, 145